# DEVELOPMENT AND SUCCESSFUL TESTING OF THE FIRST $Nb_3Sn$ WOUND, IN SITU-REACTED, HIGH-FIELD SUPERCONDUCTING QUADRUPOLE OF CERN

A. Asner, C. Becquet, H. Rieder, C. Niqueletto and W. Thomi
CERN, Geneva, Switzerland

## Abstract

Following an extensive development of the "wind and react" technology of high-field and high-current density, Cu-stabilized $Nb_3Sn$ cables, a sizeable, 1 m long, 9 cm bore, 100 KJ superconducting quadrupole magnet has been built and successfully tested and operated. Specific technological and design aspects of this magnet will be described, such as the simultaneous reaction process and heat treatment of the quartz insulation and solutions to problems of interconnections, the coil manufacture and the assembly of the active part of the magnet given. The quadrupole has been successfully tested and operated. The maximum current of 1.1 kA corresponds to an overall current density over the cross-section of the insulated cable of 3 x $10^4$ A/cm$^2$ at a maximum field of 8 T (within 0.2 T) and was reached after only 5 quenches. These figures correspond to 93-99% of the critical current densities, measured on cable samples, reacted with each pole winding of the quadrupole. The nominal current of 1 kA was reached without quench and repeatedly maintained for several days. We believe that this new technology and the successful development of the first high-field, $Nb_3Sn$-cable-wound quadrupole magnet of CERN open new and exciting possibilities for the development of accelerator and storage ring high-field dipole magnets in the 10 T range with stored energies of 1 MJ per metre of length.

## 1. Introduction

In a paper presented at the 1980 Applied Superconductivity Conference at Santa Fe[1] the preparatory activity and the initial phase of the realization of the first 1 m long, 9 cm bore high-field quadrupole of CERN, wound with a $Nb_3Sn$ cable and reacted *in situ* after winding was described.

This quadrupole has now been manufactured, successfully tested, and operated. A maximum field of ≃ 8 T has been obtained for the first time in a high-field and high-current density superconducting magnet, confirming the effectiveness of the novel and complex technology for the realization of $Nb_3Sn$ wound magnets. Design parameters were reached and a reliable, fully operational, high-precision quadrupole was made for a beam of secondary particles at CERN.

Let us briefly recall the preparatory activities: as a result of development efforts in the USA, Europe, and Japan, Cu-stabilized filamentary $Nb_3Sn$ superconductors became available in the late 1970's. Owing to the high critical temperature of $Nb_3Sn$, $T_c$ = 18 K at B = 0 T and to its high $j_c$ and $B_{c2}$ values, the available temperature margin with respect to the coolant temperature

$$\delta T = (T_c - T_0)\left[1-\left(\frac{I_n B_n}{I_c B_c}\right)^{0.5}\right] \text{ (K)} \qquad (1)$$

offers, in the 8-10 T field range, comparable $\delta T$'s to the NbTi superconductor at 4-5 T.

Manuscript received November 30, 1982

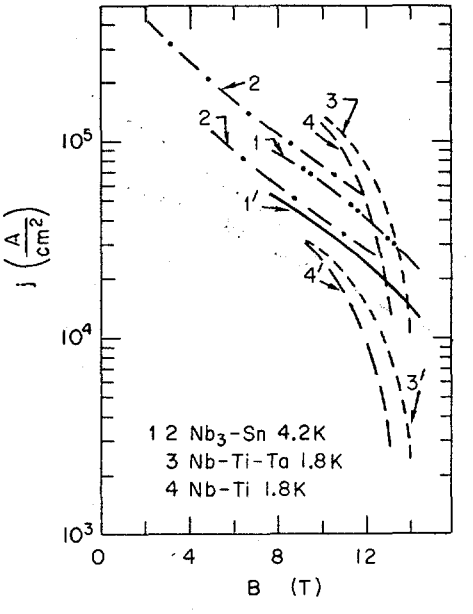


Fig. 1 Overall current density curves for the $Nb_3Sn$ cable according to the bronze 1 resp. external diffusion process 2, without and with insulation 1', 2'. Curves 3 and 4 refer to NbTiTa and NbTi cables at 1.8 K and curves 3' and 4' to the same insulated cables with 30% volume of helium in it.

The use of $Nb_3Sn$ superconductors thus represents one line of action towards the development of high-field magnets for future particle accelerators and storage rings, the other line being the use of NBTi or NbTiTa-wound magnets cooled with superfluid He II to 1.8-1.9 K. The respective $j_c = f(B_c)$ curves for these superconductors are shown in Fig. 1.

The decision to build the quadrupole followed the successful development and testing of a 2.3/9.0 cm Ø, 5 cm long solenoid, wound with a 1.1 x 2.2 mm$^2$ cable made by Vacuumschmelze in Germany; the cable is shown in Fig. 2. By designing, manufacturing, and testing the solenoid, valuable experience has been gained in handling the delicate and brittle superconductor and in solving problems of insulation, of reaction, and of the winding connections.

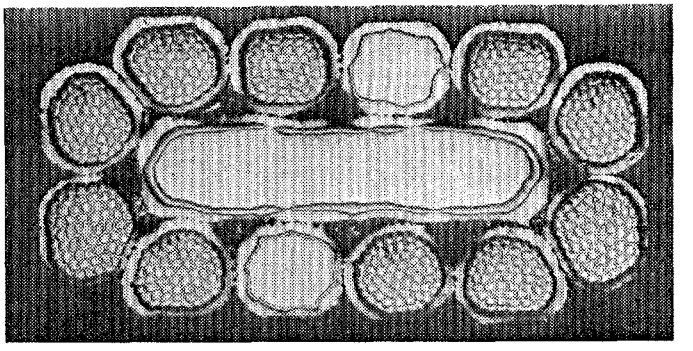

Fig. 2 1.1 x 2.2 mm$^2$ $Nb_3Sn$ cable, made of three stabilizing copper elements and of ten 0.4 mm Ø niobium and bronze composites

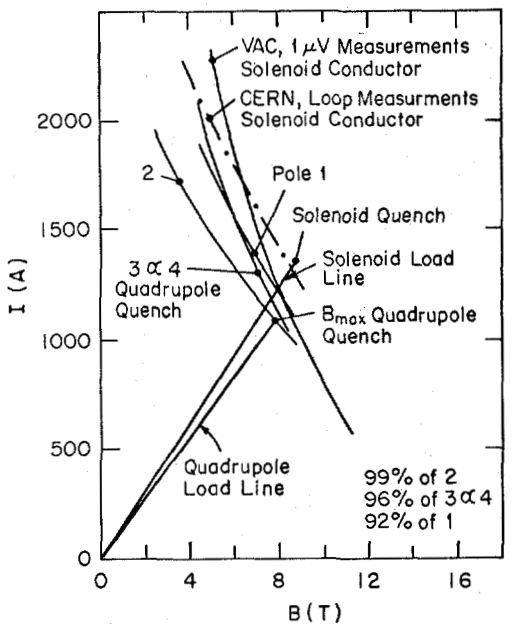


Fig. 3 Results of short sample measurements for solenoid and quadrupole $Nb_3Sn$ cables and load lines

Figure 3 shows the results obtained: at a current of $I_c$ = 1370 A a field of 8.8 T has been achieved; the current density over the cable cross-section was 5.64 x $10^4$ A/cm$^2$ and over the insulated cable it was 3.52 x $10^4$ A/cm$^2$ (see Fig. 2). These values lie beyond the measured short sample curve of the cable, most probably owing to the known stress relieving effect of bronze[2] under the influence of hoop stresses in the winding.

## 2. Mechanical design of the quadrupole

The mechanical design is largely based on CERN's now more than 10 year's experience in developing NbTi-wound superconducting beam-transport magnets, following the concentric, coaxial design with a split and "cold" iron for field enhancement, as first applied by Leroy[3]. In 1971 the 1 m long, 9 cm bore quadrupole "Castor" was built, followed by the two 2.3 m long, 500 kJ dipoles of the CEA-Saclay-CERN collaboration[4,5] and by the eight low-β section quadrupoles for the CERN Intersecting Storage Rings[6]. All these magnets were designed according to the above method, and are performing very satisfactorily. Figure 4 shows the cross-section of the active part of the $Nb_3Sn$ quadrupole. The elements of the active part are

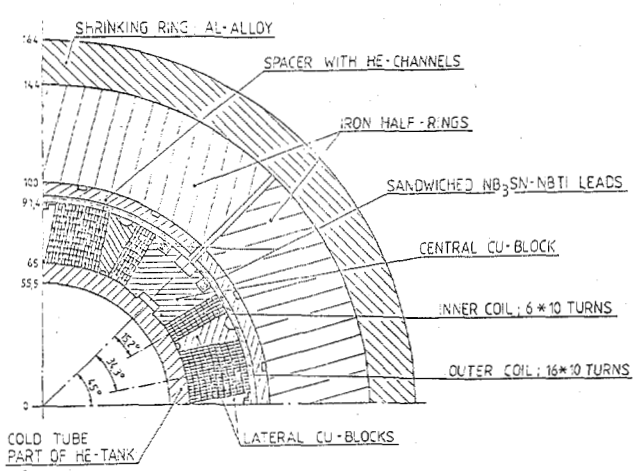


Fig. 4 Cross-section of the 1 m long, 9 cm warm bore superconducting quadrupole, wound with the $Nb_3Sn$ cable of Fig. 2

assembled around the central, 10 mm thick cylinder of 316 NL-stainless steel, which has circumferential channels for cooling. Following this are four pole windings, wound around the precisely machined central Cu "poles" and wedges. Four ventronite-clad, stainless-steel segments with channels for helium flow are placed around the coils, followed by the two half-rings of soft magnetic iron. At the ends the soft iron half-rings are replaced by stainless-steel ones. An external clamping ring of slightly reduced inner diameter, made of Al alloy, is heated and shrunk around the iron halves.

The iron thus acts as a transmitter of force to the winding. Taking into account the elastic moduli E (kg/mm$^2$), the coefficients α ($K^{-1}$) of the thermal contraction between 300 K and 4.2 K, and the geometry of the different components, the main requirements to be met for a safe mechanical design are: at room temperature and at 4.2 K, without and with applied electromagnetic forces, the windings must be under radial and azimuthal compression; the azimuthal and radial stresses σ and $P_r$ (kg/cm$^2$) must everywhere, and notably in the impregnated winding, remain within the limiting values, as measured on adequate samples.

In the longitudinal, axial direction, special Cu segments are placed at the coil ends, and axial pressure is exercised by means of spring-loaded screws, fixed to the inner stainless-steel tube. This arrangement compensates the differential thermal contraction between the stainless-steel tube and the winding, and counterbalances to a certain extent the influence of the electromagnetic forces in the coil-ends, keeping the tensile stresses there within allowed limits.

Table 1 shows the radial and normal, i.e. azimuthal, stresses in the various parts of the quadrupole at a resulting outward-directed electromagnetic force of 200 (t/m) and an axial force in the coil ends of 27 t.

Table 1

Stresses in the elements of the active parts

| Element | Cool-down from 300 K to 4.2 K | | Cool-down plus electromagnetic forces | |
|---|---|---|---|---|
| | σ (kg/mm$^2$) | $P_r$ (kg/mm$^2$) | σ (kg/mm$^2$) | $P_r$ (kg/mm$^2$) |
| Inner tube | -8.6 | -1.1 | -12.9 | -2.9 |
| Impregnated winding | -6.3 | -1.7 | - 2.0 | -0.5 |
| Outer clamping ring | 7.0 | 1.0 | 10.0 | +2.0 |
| Longitudinal stress in the winding | -0.75 | | 3.0 | |

## 3. Coil Manufacturing and Assembly

It is evident that the coil manufacturing and the assembly of the active part had to be subordinated to the imperatives of the "wind and react" technology of the $Nb_3Sn$ superconductor. For the quadrupole magnet the same cable as for the solenoid was used; according to Fig. 2 the cable consists of ten 0.4 mm Ø $Nb_3Sn$ plus bronze composites, cabled with two 0.4 mm Ø Cu wires around a central 1.5 x 0.4 mm$^2$ Cu strip. All Cu-stabilizing elements, about 33% of the cable cross-section[7], were surrounded by a Ta barrier and by a second Cu layer covered with tin on its outside.

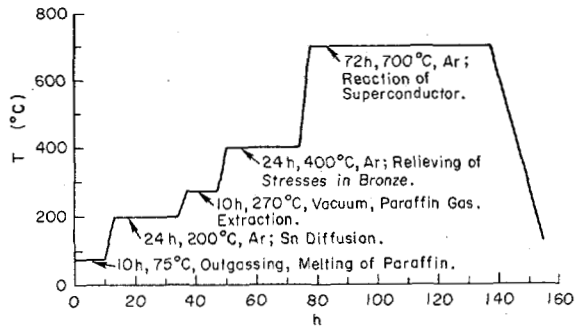


Fig. 5 Heat treatment process for the $Nb_3Sn$ cable and the insulation

The 0.25 mm one-sided quartz insulation woven around the cable has a low carbon content. The insulated cable is "soaked" in a 50% solution of paraffin. Figure 5 shows the temperatures of the combined process of paraffin extraction, Sn diffusion, bronze stress-relieving, and of the $Nb_3Sn$ reaction, as for the bronze technique.

The coil winding and reaction process will now be described. Each pole winding of 6 and 16 layers with 10 turns each is wound on a precisely machined stainless-steel cylinder. During the entire winding process, inter-turn and ground insulation were carefully monitored and registered. The central and lateral $Al_2O_3$-insulated Cu pieces were fixed to the winding mandrel (Fig. 6). The Cu elements are split longitudinally to allow for differential thermal expansion and contraction between the winding and the supporting structure during reaction and impregnation.

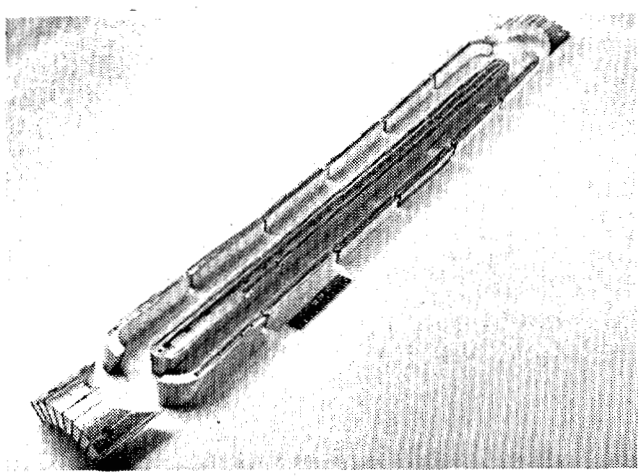

Fig. 6 $Al_2O_3$-insulated central, lateral, and end blocks of copper for a pole winding

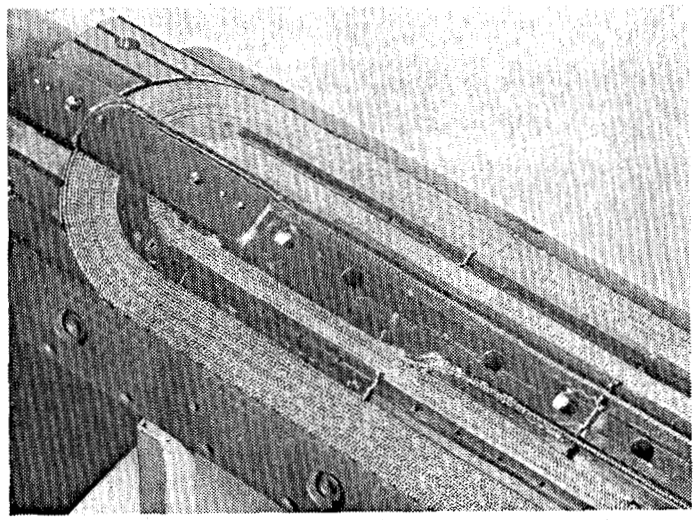

Fig. 7 View of a pole winding before the reaction process

The winding was terminated and the Cu end-blocks put in place (Fig. 7). The lateral stainless-steel bars and grids were added with a certain clearance to confine the coil, which was then transported to the reaction oven. After the reaction, additional glass-fibre and kapton ground insulation was applied and each $Nb_3Sn$ conductor end sandwiched between two NbTi conductors and indium-soldered (Fig. 8). The coil was

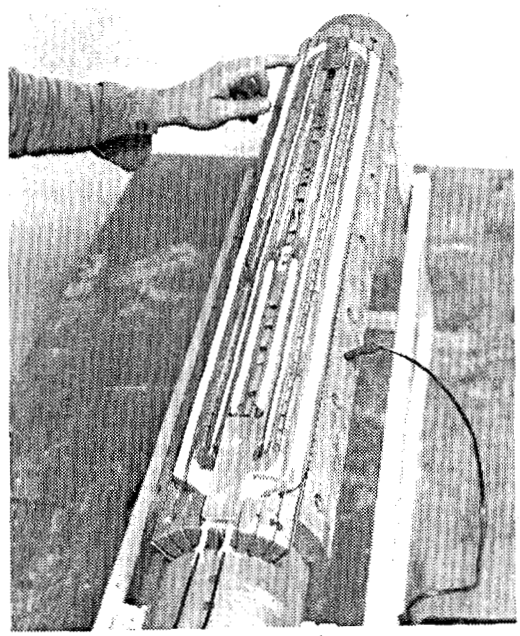

Fig. 8 Preparation of the coil for impregnation: soldering of the NbTi-$Nb_3Sn$ end connections and application of ground insulation.

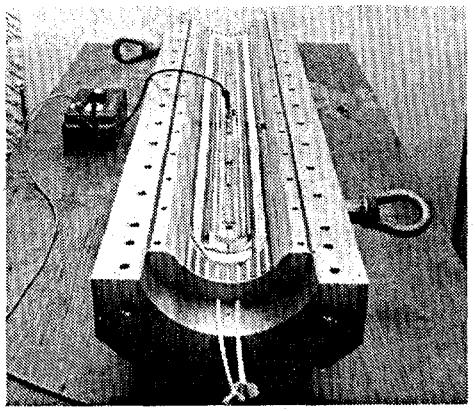

Fig. 9 Coil placed into precise impregnation mould for vacuum and pressure impregnation

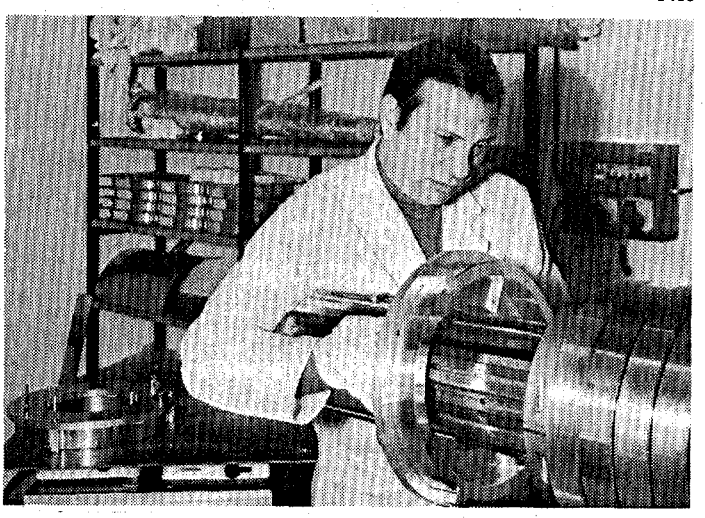

Fig. 11 Mounting of the 160°C heated outer clamping rings of Al alloy

then placed with its external surface in a precisely-machined impregnation mould (Fig. 9) which tightly confines the winding and determines its very precise geometry. Figures 10 and 11 show the mounting of the iron halves with the stainless-steel segments and the shrinking of the hot Al alloy rings, while Fig. 12 shows the active part of the magnet with the pole-winding inter-connections and the mounted precooling jacket.

After assembly in its cryostat, consisting of a helium, a liquid-nitrogen and a vacuum vessel, the addition of a second thin iron screen around it, the quadrupole was installed in the test laboratory by May 1981.

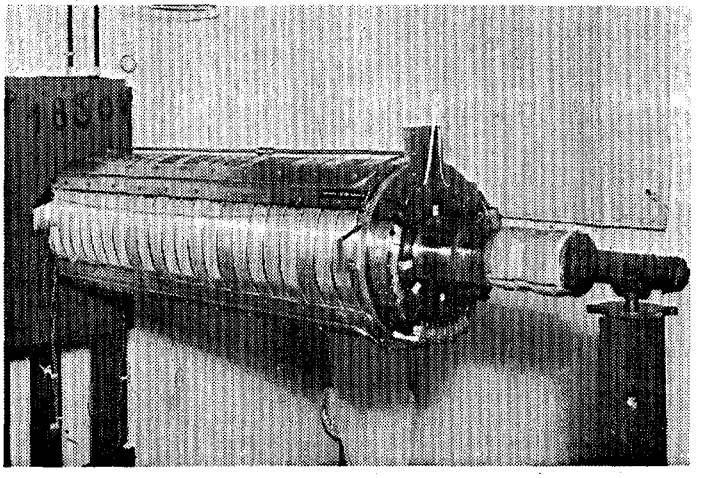

Fig. 12 View of the assembled active part with inter-connections between pole windings and the LN-precooling jacket

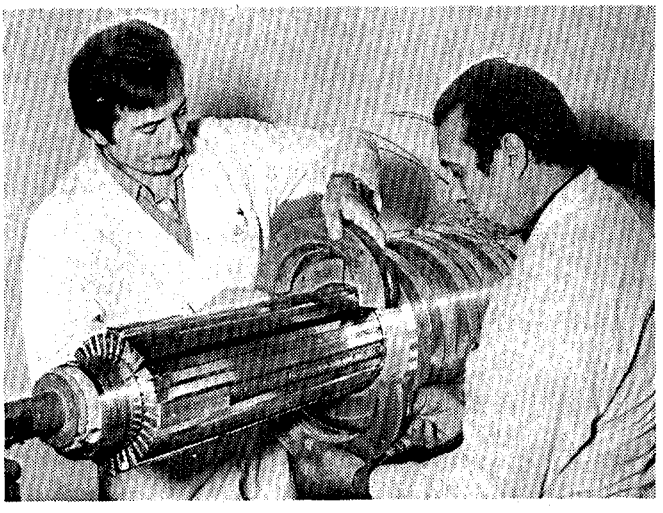

Fig. 10 Mounting of the split soft-iron half-rings around the four coils

## 4. Test Results

During the cool-down process and during the transition of the four coils to superconductive state, the resistance and voltage drop across the sandwiched NbTi-$Nb_3Sn$ connections were measured. Comfortably low values of 2 to 5 x $10^{-8}$ Ω for ≃ 10 $cm^2$ contact surface were measured, independently of the excitation current.

The current in the quadrupole was then raised to 1 kA where the first quench occurred. In four subsequent quenches the current reached $I_{max}$ = 1.1 kA. The corresponding field gradient in the quadrupole was G = 70.5 T/m and the maximum field in the coil-ends was $B_{max}$ = 7.8 ± 0.2 T; the corresponding overall current density was $j_{max}$ = 3 x $10^9$ $A/cm^2$. As indicated in Fig. 3 these figures correspond to 93-99% of the critical currents, measured on short samples cut from every pole-winding conductor and reacted with its coil.

Two out of the five quenches were rather strong and voltages up to 250 V were registered across individual pole windings. It should be stated that the quadrupole had no protecting, energy-discharge resistors during the first run. The quadrupole was then opened, inspected, and equipped with a 0.2 Ω discharge resistance, each pole being connected in parallel to

0.05 Ω. The second run took place early this year. The magnet was repeatedly excited to 1 kA without any training or quench, operated during two weeks, and magnetic measurements were performed. The only quench occurred at $I_m \simeq 1.1$ kA, when the voltages across the poles remained below 17 V. Within 300 s after this quench the magnet was excited to 1 kA (see Fig. 13).

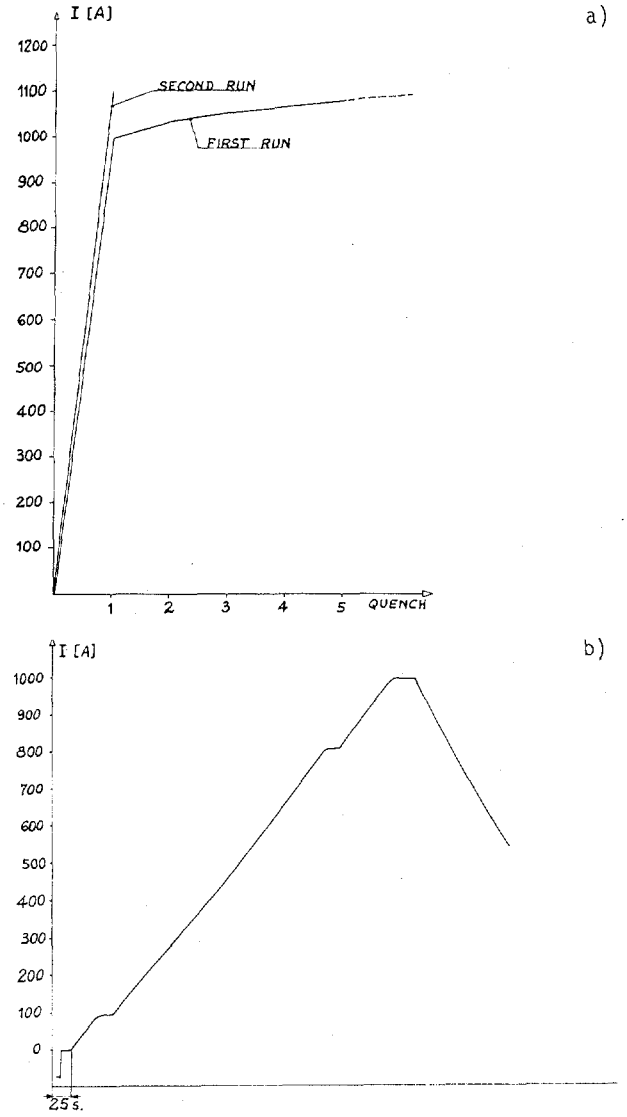


Fig. 13 Quenches of the $Nb_3Sn$ wound quadrupole, followed by excitation to nominal current of $I_n$=1100 A

Table 2 gives a summary of the main quadrupole parameters; the excellent cryogenic performance of the quadrupole is stressed.

Table 2

Main parameters of the $NB_3Sn$ quadrupole of CERN

| Parameter | | Nominal | Maximal |
|---|---|---|---|
| Magnetic length | $\ell$ (m) | 0.9 | 0.9 |
| Warm bore diameter | d (cm) | 9.0 | 9.0 |
| Current | I (A) | 1005 | 1100 |
| Current density | j (A/cm$^2$) | $2.7 \times 10^4$ | $3 \times 10^4$ |
| Max. field in coil end | $B_{max}$ (T) | 7.2 | $7.8 \pm 0.2$ |
| Useful bore field gradient | G (T/m) | 64.0 | 70.5 |
| Stored energy | E (kWs) | 92 | 100 |
| Heat losses | H (W) | 5 | 5.5 |
| Vacuum | P (Torr) | $\sim 10^{-8}$ | $\sim 10^{-8}$ |
| Field linearity error within useful aperture | $\frac{\Delta B_6}{B_0}$ | $= -5 \times 10^{-4}$ | |
| | $\frac{\Delta B_{10}}{B_0}$ | $= 2 \times 10^{-4}$ | |
| | $\frac{\Delta B_{12}}{B_0}$ | $= -7 \times 10^{-4}$ | |

## 5. Conclusions

The successful development, testing, and operation of the first high-precision, high-field, $Nb_3Sn$ wound quadrupole magnet of CERN has confirmed the choice and implementation of the "wind and react" technology. Valuable experience in handling the reliable $Nb_3Sn$ superconductor has been gained. Future improvements, notably the development of adequate insulating materials of improved mechanical and dielectric strength, also after the high-temperature reaction process, would be very helpful, as quartz fibres represent one among several insulations that could be applied.

As to the $Nb_3Sn$ superconductor, the main disadvantage of the two processes available today, the "bronze process" and the external Sn diffusion one, is the high, roughly 50% bronze content remaining in the final composite. The average overall current density and/or the amount of the copper stabilizer are thus reduced and a good part of the performance of the superconducting filaments lost.

Following the development of the $Nb_3Sn$ quadrupole, it would be of obvious interest to develop a 9-10 T high-field dipole magnet along the same lines, in order to see whether problems related to the much higher stored energies and forces can be solved and whether such magnets could be built for future particle accelerators and storage rings in the multi-TeV range.

At CERN, a preliminary design was made and computations performed which are briefly summarized here. The main parameters of a 9 T bore field dipole wound with a 2.0 x 14.5/2.5 x 15 mm$^2$ $Nb_3Sn$ cable reacted after winding are summarized in Table 3.

The winding has four layers. Around the inner tubes of titanium, the two layers of the inner winding are placed, each layer consisting of four blocks in between adequate "poles" and wedges. An intermediate ring of stainless steel is placed around the inner winding, followed by the two layers of the outer coils and by the second intermediate stainless-steel ring. The

first, thin, split "cold" iron screen halves are placed around this ring and the whole cold active part is tightened by the Al alloy shrink rings. The second, concentric iron screen is at room temperature. The free space is foreseen for the forced-flow cryostat elements and for an adequate suspension system between the active part and the outer Fe screen.

Figure 14 shows the computed stresses in the various blocks of the inner and outer windings. Despite the very considerable electromagnetic and thermal contraction forces, the stresses in the windings and in the active part can be kept within reasonable and tolerable limits.

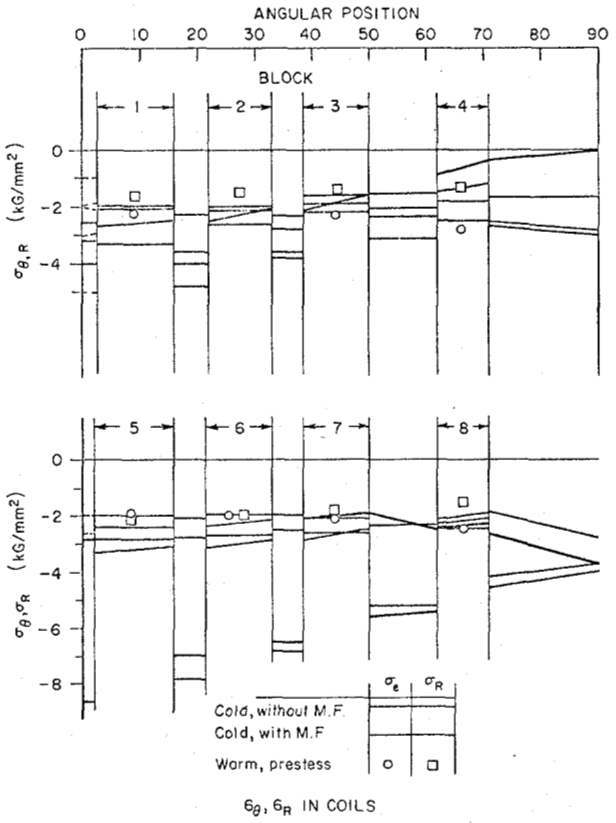


Fig. 14 Stresses in the various blocks of the inner and outer windings

## APPENDIX

### Determination of the magnetic end-field in superconducting quadrupole and dipole magnets

In this Appendix a method is presented for the determination of the end-field, which coincides with the highest field appearing in a superconducting quadrupole or dipole magnet; the method is based on analytical expressions and the application of known 2D-computer programs for magnetic fields such as the "Poisson". The method is preferred to direct measurements with Hall plates. In the case of the present $Nb_3Sn$ quadrupole the inner coil radius in the end part is $\simeq$ 1.2 cm and the maximum field appears at that radius; a 6 x 2 mm² Hall plate would at best measure a field 3 mm away, vertical and radial positioning tolerances excluded.

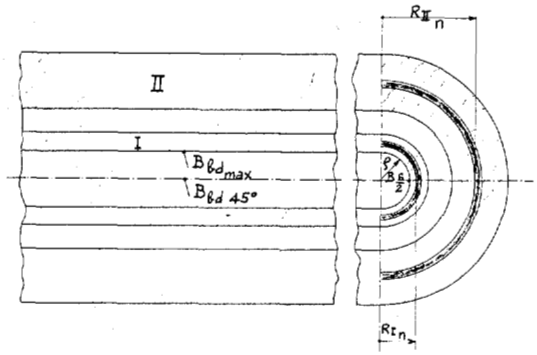


Fig. 15 End field computation; decomposition of the quadrupole end field into a linear and half-solenoid part

In accordance with Fig. 15, it is assumed that the end-field has two components: a "linear" one due to the left, straight bidimensional field of 0.5 $B_{bd}$ (T) and a second one due to the multiblock and multilayer half-solenoidal field $B_{s/2}$ (T):

$$B_{end} = 0.5\ B_{bd} + B_{s/2}\ (T). \qquad (2)$$

The linear component is obtained from computer programs such as "Poisson"; two values are of interest $B_{bd}$ and $B_{bd\,max}$ (see Fig. 16a), along the 45° symmetry line of the quadrupole (90° for a dipole), and the maximum field in the linear part, appearing along the inner surface of the smallest, innermost block of the winding. In the case of the $Nb_3Sn$ quadrupole the corresponding fields for $I_{max}$ = 1.1 kA and $j_{max}$ = 3 x $10^9$ A/cm² are $B_{bd\,max}$ = 6.25 T and $B_{bd}$ = 5.2 T.

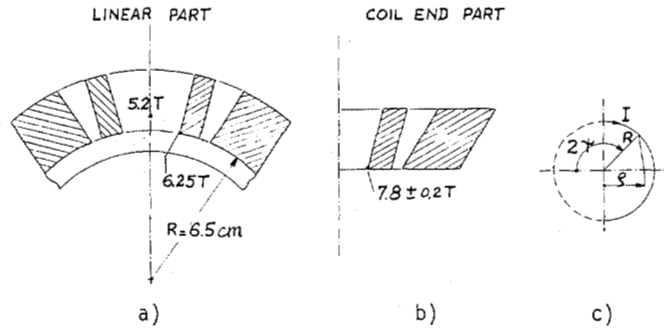


Fig. 16 Magnetic field values obtained in the straight and end parts of the $Nb_3Sn$ wound quadrupole at maximum current of $I_{max}$ = 1100 A

To find $B_{s/2}$ one needs to know the expression for a field of $B_s$ of a corresponding full solenoid and to determine the ratio of $\xi = B_{s/2}/B_s$; $B_s$ can easily be obtained by computer programs for solenoid fields. The factor $\xi$ is obtained as follows: from Fig. 16c, one can write for the field $B_s$ at a distance $\rho$ and due to the current I flowing in an infinitely thin loop of radius R:

$$B_s = -\frac{\mu_0 I}{\pi(R+\rho)} \int_{\pi/2}^{0} \frac{d\psi}{\sqrt{1-k^2\sin^2\psi}}$$

$$= \frac{\mu_0 I}{\pi(R+\rho)} F(\pi/2,\alpha) \qquad (3)$$

and for a half loop

$$B_{s/2} = \frac{-\mu_0 I}{\pi(R+\rho)} \int_{\pi/2}^{\pi/4} \frac{d\psi}{\sqrt{1-k^2\sin^2\psi}}$$

$$= \frac{\mu_0 I}{\pi(R+\rho)}\left[F(\pi/2,\alpha) - F(\pi/4,\alpha)\right] \qquad (4)$$

with

$$k = \frac{2\sqrt{R+\rho}}{R+\rho} \qquad (5)$$

$$\alpha = \arcsin k \qquad (6)$$

$$\xi(R,\rho) = \frac{B_{s/2}}{B_s} = \frac{F(\pi/2,\alpha) - F(\pi/4,\alpha)}{F(\pi/2,\alpha)} \qquad (7)$$

to be determined from Jahnke-Emde tables of elliptic functions[8]. In practice, however, one has to deal with coils of infinite width. One also has to avoid singularities for $B_{s/2} \blacksquare B_s = \infty$ at $\rho = R$. The practical approach is then as follows:

i) the field map of the end-field configuration is computed, e.g. by the "Poisson" program, assuming a multiconcentric, full solenoid configuration;

ii) the coil blocks are sliced and the corresponding $\xi_1 \ldots \xi_n$ values are computed for the n slices at $\rho_n$, the relevant $\xi$ is then:

$$\xi = \frac{1}{n}\sum_{1}^{n} \xi_n \; ; \qquad (8)$$

iii) the final $B_{s/2}$ is then equal to the sum of the contributions of each half coil at $\rho = \rho_n$ (Fig. 16b).

In the case of a quadrupole magnet one has, in addition, to establish the field coupling factor between one and four coil-ends. It is assumed that the coupling is the same as for the straight, linear part, which is easily obtained from two computer runs, one for a single pole and one for four poles.

For the superconducting $Nb_3Sn$ quadrupole one obtains for I = 1.1 kA:

$B_{s/2}$ = 2.25 + 2.8 = 5.05 T

0.5 $B_{bd\ max}$ = 2.95 T

0.5 $B_{bd\ 45°}$ = 2.6 T

yielding

$B_{max}$ = 7.8 ± 0.2 T.

$B_{bd\ max}$ and $B_{bd\ 45°}$ are the arithmetic mean of the values obtained with and without the Fe screen.

Acknowledgements

Fruitful discussions with Messrs. D. Leroy and D. Hagedorn are acknowledged.

References

1. A. Asner et al., "Development and testing of high field, high current density solenoids and magnets, wound with stabilized filamentary $Nb_3Sn$ cable and reacted after winding", IEEE Trans. Magn., Vol. MAG-17, No. 1, p. 416-9, January 1981.

2. G. Rupp, "Improvement of the critical current of multifilamentary $Nb_3Sn$ conductors under tensile stress", IEEE Trans. Magn., Vol. MAG-13, No. 5, pp. 1565-7, September 1977.

3. A. Asner and A. Leroy, "A low stored energy, high precision superconducting quadrupole for high energy beams", Proc. 1972 Int. Conf. on Magnet Technology, Brookhaven, USA, USAEC CONF 720908, pp. 164-6, 1973.

4. J. Perot and D. Leroy, "The Superconducting bending magnets CESAR", Proc. 1977 Int. Conf. on Magnet Technology, Bratislava, Czechoslovakia, ALFA, pp. 487-91, 1978.

5. J. Perot and D. Leroy, "Tests of the superconducting bending magnets CESAR", IEEE Trans. Magn., Vol. MAG-15, No. 1, pp. 100-2, January 1979.

6. J. Billan et al., "The eight superconducting quadrupoles for the ISR high luminosity insertion", report CERN-IRS-BOM-GE 80/22 (1980).

7. M. Wilson (Rutherford Lab.), "Proportion of copper in $Nb_3Sn$ composites" in Fourth Course on Solar Energy Conversion, Trieste, 1977, ICTP report SMR/36 (1978).

8. E. Jahnke and F. Emde, Tables of higher functions, 6th ed., revised by F. Losch, Stuttgart: Teubner, 1960.